A simple method for identifying the elementary units governing the mechanical properties in leather materials

Wenjun Long[1], Liangqiong Peng[1], Jiheng Li[1], Yue Yu[1*] and Wenhua Zhang[1,2*]

Abstract

Understanding the mechanical properties of leather is crucial for expanding its range of application, but the influence of collagen fibril bundles (FBs) remains unclear. In this study, 12 kinds of bovine leather were prepared with varying FB sizes using Cr(III), Zr(IV) and aldehyde as the crosslinking agents along with different fillers such as rapeseed oil phosphate, polyacrylic acid and their combination. The experimental results revealed that the tear strength of leather was affected by the crosslinking agents, which could be further adjusted by the filler. Accordingly, a simple method using mercury intrusion porosimetry has been proposed for determining the FB size based on the crack-bridging model. Specifically, the tear strength of leather showed a strong correlation with the FB radius where the strength increased with the decrease in FB radius. This indicated that FBs served as the elementary units contributing to loading strength. These findings may facilitate the development of cleaner technologies for fabricating high-performance leather through the regulation of FB size.

Keywords Leather, Fibril bundles, Mechanical properties, Dispersion, Aggregation

*Correspondence:
Yue Yu
yuyue@scu.edu.cn
Wenhua Zhang
zhangwh@scu.edu.cn
Full list of author information is available at the end of the article

Graphical abstract

1 Introduction

The processing–structure–property–performance framework is a crucial design methodology in materials science and engineering [1]. However, the complexity of the leather-making process makes it difficult to understand how the microstructure of skin collagen fibers imparts the necessary mechanical properties into leather. Leather is usually made from natural animal skin, which is a by-product of the meat industry, and it primarily consists of protein type I collagen. During the tanning process, crosslinking agents such as inorganic Cr(III) and Zr(IV) complex or aldehyde form coordinate or covalent bonds with the functional groups of collagen, effectively stabilizing the fibrous structure of the skin and enhancing the mechanical properties [2, 3]. During the post-tanning process, the leather performance can be further improved by adding retanning agents and fatliquors that interact with collagen via weak electrostatic interaction, hydrophobic interaction or hydrogen bonding [4, 5]. Leather inevitably contains a significant amount of post-tanning chemicals (5–20%) such as retanning agents and fatliquors, which pose a hazardous risk. Consequently, various cleaner technologies have been explored to obtain leather with desirable performance characteristics, and most of the previous studies have focused on the tanning chemistry, including the development of developing innovative organic or inorganic crosslinking agents for tanning or using alternative chemicals to stabilize the pelt for post-tanning process [2]. Controlling the mechanical properties of leather such as its tensile strength, tear strength and softness is critical for a wide range of applications such as traditional furniture, clothing and novel functional materials like on-skin devices and electromagnetic interference shielding [6, 7].

In leather industry, the tanning and post-tanning processes are typically considered to be essential for producing stronger leather with better handling performance. However, He et al. found that collagen fibers could be greatly strengthened merely by adjusting their dispersion through dehydration using an organic solvent without the need for crosslinking [8]. This indicates that the complex tanning and post-tanning processes may not be necessary for improving the mechanical properties of leather. The multiple steps involved in the tanning and gradient dehydration processes can alter the microstructure of skin fibers in a similar manner. Thus, exploring the microstructural changes during the tanning and post-tanning processes can aid in designing leather materials for different applications.

The leather-making process removes nonstructural components from natural skin, such as dirt, hair, epidermis, fat, veins and flesh, which leaves behind a fibrous collagen network that can be easily observed using low-resolution light microscopy [9]. This network consists of numerous fibril bundles (FBs) with varying diameters, positioning FBs as a substructural unit of fiber. As shown in Fig. 1, fibrils characterized by their D-periodic banding pattern represent the smallest structural unit that can be observed by electron microscopy. Fibrils are formed by the aggregation of collagen molecules, and their D-spacing covers two regions: gap and overlap regions [9].

Several researchers have examined the key factors influencing the mechanical properties of leather, such as the chemistry of the tanning and post-tanning processes [3, 10] and fiber radii [11]. Various technologies have been employed to measure the fibril diameter including transmission electron microscopy (TEM) [12], atomic force microscopy (AFM) [13, 14] and small-angle X-ray scattering (SAXS) [15]. Notably, larger fibril diameters have been found in stronger tissues, such as mouse tendons and human aortic valves, which indicates a correlation between larger diameters and higher strength [16–18]. However, other studies, which used spun raw materials to construct a series of collagen fibers with physically controlled fiber diameter, showed that smaller fiber diameters can yield higher tensile strength [11, 19–21]. These conflicting trends indicate a discrepancy between natural tissue and artificial material, which underscores the need to explore the hierarchical structure of collagen fibers for understanding their mechanical behavior. This is particularly important for leather, which is obtained by processing natural skin collagen fibers. However, only few studies have focused on the effects of microstructure on its mechanical properties. Wells et al. [15] utilized SAXS to investigate the mechanical properties of leather and found no significant correlations between the fibril diameter and mechanical properties, suggesting that the elementary unit for mechanical properties differs from the elementary structural unit (e.g., fibrils). Identifying the true elementary unit influencing the mechanical properties is of immense significance for fabricating innovative leather materials through collagen fiber control.

Leather's unique porosity contributes to its hygiene properties, and these pores exist among FBs as well as fibrils with various pore sizes. Thus, it is reasonable to infer that FBs play a critical role in the mechanical properties of leather. He et al. [22] used mercury intrusion porosimetry (MIP) to show that the tensile stress applied to leather was positively correlated with its porosity. MIP can provide the pore size distribution of the entire sample in single measurement after a simple pretreatment, facilitating robust statistical analysis while minimizing the sampling errors and experimenter bias present in techniques such as scanning electron microscopy [23]. MIP can effectively detect pore sizes in the range of 6–300,000 nm, encompassing nearly all pores among FBs. Notably, MIP can be used to determine the total pore size and surface area per unit leather mass by fitting the measurements to a cylindrical pore model. Then, the pore size distribution can be used to calculate the FB size distribution.

This study explores the relationship between the FB size and tear strength to identify the elementary unit governing the mechanical properties of leather. Twelve types of leather samples with different microstructures have been prepared and characterized by a series of spectroscopic technologies. Furthermore, a simple method is proposed for measuring FB radii using MIP, and the crack-bridging model is employed to establish a quantitative correlation between the tear strength of leather and the FB radius. The findings of this study provide useful insights into the development of cleaner technologies for fabricating high-performance leather through the regulation of FB size.
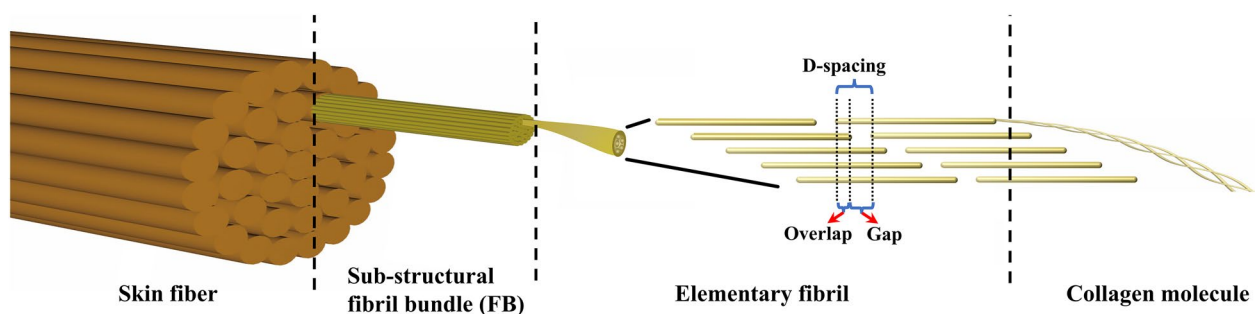
Fig. 1 Hierarchical fibrous structure of leather

2 Materials and methods

2.1 Sample preparation

Raw bovine skins were purchased and pretreated to retain only the collagen fibers. For the tanning process, three different crosslinking agents were employed to stabilize and disperse the raw skin fibers (Table S1): a typical macromolecular organic aldehyde (TWS), inorganic $Cr_2(SO_4)_3$ Cr(III) and biomass-derived hydroxycarboxylic acid zirconium complexes (Zr(IV)). The samples prepared with these crosslinking agents were labeled as TWS-, Cr- and Zr-leathers. To minimize heterogeneity, samples were taken symmetrically along the midline of the skins (Fig. S1).

In the post-tanning process, three different fillers were used to regulate the fiber structure: hydrophobic rapeseed oil phosphate (OP), hydrophilic polyacrylic acid (PA) and a combination of OP and PA (OA) (Table S2). Thus, nine types of leather were obtained after the post-tanning process. All samples including blanks from the tanning process were dried at 35 °C by using a stretch dryer (BBS 2700, China) and softened with a vibration staking machine (GLRZ1-1600, China). In total, 12 types of leather materials were obtained.

TWS, Zr(IV), OP and OA were of industrial grade and supplied by Tingjiang Co., Ltd., China. The other reagents were of analytical grade and supplied by CHRON Co., Ltd., China.

2.2 Strength test

The tear strength (TS) was measured by using the standard method [24]. All samples were kept at a temperature of 20 °C and humidity of 65% for 48 h. Then, rectangles were cut from each sample in duplicate (Fig. S1b), and the thickness of the cracking extension edge was recorded using a digital thickness meter (My-3130-a2, China) (Fig. S1c). TS was determined using an AI-7000 servo control system machine (Gotech Testing Machines Co., Ltd., China) operating at a uniaxial elongation rate of 100 mm/min.

2.3 Structural characterization

Scanning electron microscopy (SEM; FEI Nova Nano SEM 450, USA) was employed to observe the sample morphology. The FB radii were estimated using the ImageJ software. The D-spacing of the fibrils was calculated by SAXS (Bruker Nanostar U SAXS, USA) using an X-ray energy of 50 kV and a wavelength of 0.154 nm. The lateral distance between collagen molecules was obtained by X-ray diffraction (XRD; Bruker D8 Advance, USA) using Cu (wavelength: 0.154 nm) and a step length of 0.02°. Attenuated total reflectance Fourier transform infrared (ATR-FTIR) spectrometry (PerkinElmer

Spectrum 3, USA) was utilized to identify the functional groups present in different leather samples. Scanning was conducted from 4000 to 650 cm^{-1} at a resolution of 4 cm^{-1}.

2.4 Calculation of the fibril bundle radius

The porosity and total pore volume of the leather samples were measured using MIP (Micromeritics AutoPore IV 9500, USA) after freeze-drying (LGJ-30F freeze dryer, China) to preserve the aggregation structure and reduce moisture content. The FB radius was calculated from the pore structure parameters. As illustrated in Fig. 1, collagen molecules with a length of 300 nm and a diameter of 1.5 nm bind together to form elementary fibrils, which are arranged into FBs that further combine to form fibers with various voids [9]. Consequently, an FB can be treated as a cylinder with a large length-to-diameter ratio. Then, the total surface area (S_f) and volume (V_f) of an FB can be expressed as follows:

$$S_f = 2\pi Rl * \rho + 4\pi R * \rho \approx 2\pi Rl * \rho \tag{1}$$

$$V_f = \pi R^2 l * \rho \approx 1/2 S_f * R \tag{2}$$

where R is the average FB radius, l is the average FB length, and ρ is the number of FBs per unit leather mass. The total pore surface area per unit leather mass (S_p) can be determined by fitting the MIP measurements to a cylindrical pore model to obtain the total surface area of FBs per unit leather mass (S_f):

$$S_p \approx S_f \tag{3}$$

The porosity (P) represents the volume fraction of pores in the leather, which is obtained from MIP measurements. Then, the total FB volume per unit leather mass (V_f) can be expressed in terms of porosity (P) and total pore volume per unit leather mass (V_p):

$$V_f = \frac{1-P}{P} V_p \tag{4}$$

Thus, the average FB radius (R) is obtained by substituting Eq. (3) into Eqs. (2) and (4) based on MIP measurements of the leather pores:

$$R = \frac{1-P}{P} \frac{2V_p}{S_p} \tag{5}$$

2.5 Crack-bridging model

As shown in Fig. 2, the tearing mechanism of fibrous materials such as cellulose nanopaper and fiber-reinforced composites can be explained by the crack-bridging model (Fig. 2) [25, 26]. The SEM images of cracked
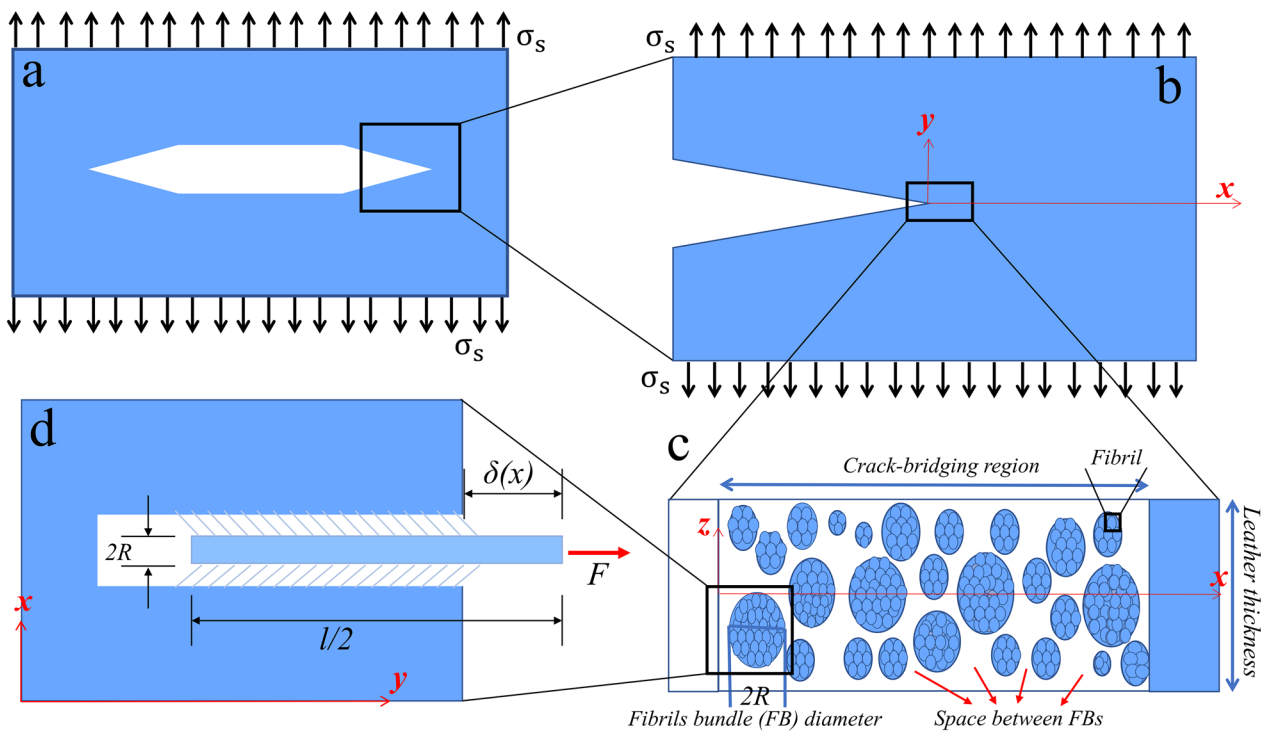
Fig. 2 Crack-bridging model for leather: **a** test model, **b** partial schematic of the test model during tearing, **c** top view of FB distribution in the torn region, and **d** force analysis diagram of a single FB during tearing

collagen fibers in the leather samples (Fig. S2) demonstrated that the FBs were pulled out during the strength test, similar to the case of nanopaper [27]. Therefore, the crack-bridging model was employed to further investigate the relationship between the FB radius and TS of collagen fibers in the leather samples. Figure 2a presents a model of the tearing of a leather sample. When a tear occurs, as depicted in Fig. 2b, the stress intensity σ_s at the tear can be expressed as follows [25]:

$$\sigma_s = \frac{V_f \tau}{R}\left(\frac{l}{2} - \delta(x)\right) \tag{6}$$

where V_f is the volume fraction of a collagen fiber, and R is the average radius of a single FB. τ represents the shear strength per unit area between FBs, which depends on their interactions. For leather samples subjected to the same tanning process, the interaction should remain constant. As shown in Fig. 2d, l is the average FB length, and $\delta(x)$ is the length of a single FB that is pulled out during the tearing process. Assuming a random distribution of FBs in the crack-bridging region, the volume fraction can be expressed in terms of the porosity P:

$$1 - P = V_f \tag{7}$$

Equation (7) can be substituted into Eq. (6) to obtain the stress intensity as

$$\sigma_s = \tau \frac{1-P}{R}\left(\frac{l}{2} - \delta(x)\right) \tag{8}$$

In the crack-bridging model, the value of $\delta(x)$ is limited to the range of 0 to $\frac{l}{2}$ [25]. When a stress is applied to a sample along the Y-axis, the crack-bridging region extends along the X-axis as shown in Fig. 2c. Assuming a uniform velocity of 100 mm/min and quasistatic crack propagation, during TS measurements, $\delta(x)$ can be approximated as constant.

The orientation index is considered uniform because samples were taken from the same regions of the bovine leather (Fig. S1a). Thus, the stress intensity (σ_s) is primarily affected by the factor $\frac{1-P}{R}$, which can be correlated with the TS obtained from experimental measurements:

$$TS = \sigma_s * k_1 = k\frac{1-P}{R} \tag{9}$$

where k_1 represents the dimensional transformation from τ (N/m^2) to TS (N/m), and k(N) is a constant reflecting the effects of the crack-bridging region, FB orientation and other factors [25, 26].

Long *et al. Collagen and Leather*   (2025) 7:6

Page 6 of 13

3 Results and discussion

3.1 Morphology

The leather samples consisted of collagen fibrils that were regulated by a crosslinking agent (TWS, Cr(III) and Zr(IV)) and a filler (OP, PA and OA), resulting in various FBs with different mechanical properties. Figure 3 shows the SEM images of the 12 different types of samples, where the FB radius is given in microns (Fig. 3m–o; detailed data in Table S3). Among the crosslinking agents, Cr(III) and Zr(IV) induce FB radii of 1–6.2 μm, while TWS leads to much larger FB radii of 3–44 μm. Among the fillers, hydrophobic OP and the blended filler OA reduce the FB radii by at least half. By contrast, hydrophilic PA nearly doubles the FB radius distributions of Cr- and Zr-leathers but has a much smaller impact on TWS. These findings indicate that different crosslinking agents and fillers result in distinct fibril aggregation behaviors in the leather.

3.2 Tear strength

Figure 4 presents the TS test results for the 12 leather samples (Fig. S3; detailed data in Table S3). Among the crosslinking agents, Cr(III) increases the TS by 20% compared with the blank sample, whereas TWS results in a slightly lower TS than Zr(IV). Thus, Cr(III) is confirmed to uniquely improve the TS of leather [28]. Using the fillers, TS was further improved by weak noncovalent interactions. The addition of hydrophobic OP significantly increases the TS, especially for Cr- and Zr-leathers (Fig. 4a, b), while the introduction of hydrophilic PA decreases TS. OA greatly improves the mechanical properties compared to Blank, especially for TWS-leather. OA also reduces the variability in the mechanical properties among different crosslinking agents. For example, Cr-leather has a TS of 75 N/mm, while Zr- and TWS-leathers have TS values of 60 N/mm and 45 N/mm, respectively. With the addition of OA, Cr- and TWS-leathers achieve TS values of approximately 83 N/mm, while Zr-leather has a TS of 70 N/mm. These findings are valuable not only for enhancing the mechanical properties but also for developing alternative eco-friendly crosslinking agents.

The mechanical properties of leather are primarily influenced by its fibrous structure comprising FBs. Notably, the aggregation behavior illustrated in Fig. 3 indicates that an increase in the FB radius is correlated with a decrease in TS as shown in Fig. 4. This trend is similar to the behavior observed in spun fiber materials [11]. For example, the TS values for Cr- and Zr-leathers follow this order: OP > OA > Blank > PA, while the FB radius follows this order: OP < OA < BlankR < PA. In the case of TWS-leather, the TS values decrease in the following order: OA > OP > PA > Blank, while the FB radius follows this order: OP < OA < PA < Blank. These results suggest that FBs serve as the elementary unit of mechanical loading.

3.3 Relationship between the fibril bundle radius and tear strength

As shown in Fig. 5a–c, the MIP results indicate that the crosslinking agents play a dominant role in determining the pore size distribution (detailed data in Table S3). For example, all the samples based on Cr-leather exhibit a pore size distribution of 1000–3000 nm. By contrast, the samples based on Zr- and TWS-leathers have similar pore size distributions exceeding 5000 nm, which are significantly larger than that for Cr-leather. Figure 5d illustrates that the fillers also affect the pore size distribution. OP decreases the average pore size of Cr-, Zr- and TWS-leathers by 25%, 35% and 50%, respectively. The addition of OA decreases the average pore size of Zr- and TWS-leathers by 30% and 58%, respectively, but has lesser impact on the Cr-leather (Table S4). However, PA increases the average pore size of Cr- and Zr-leathers by 9% and 56%, respectively, but decreases that of TWS-leather by 41%. These results clearly demonstrate that different fillers significantly impact the average pore size of TWS-leather.

The addition of crosslinking agents and fillers restructures the pores of the leather samples, affecting the fibril aggregation behavior in various FBs. Based on the porosity, pore volume and pore surface area measurements obtained by MIP, the FB radii of the 12 leather samples were estimated using Eq. (5). As shown in Fig. 5e, the FB radius ranges from 230 to 950 nm. A large discrepancy in FB radii is observed between the inorganic and organic crosslinking agents: Cr(III) results in the smallest FB radius of 424 nm, whereas TWS yields the largest FB radius of 951 nm.

Importantly, the addition of either hydrophobic or hydrophilic fillers always decreases the FB radius of Cr-leather and TWS-leather. By contrast, the addition of hydrophilic PA significantly increases the average FB radius of Zr-leather by 90%, which is correlated with the sharp decline in TS. Interestingly, the blended filler OA reduces the discrepancy in FB radii caused by different crosslinking agents, indicating that the structure of natural skin collagen fibers can be controlled in various ways.

Leather samples with a smaller pore radius exhibit a higher TS [8, 11]. However, a small pore radius does not directly guarantee a better mechanical performance, making it essential to explore the underlying mechanisms. As illustrated in Fig. 5f, the average FB radius exhibits a strong linear correlation with the average pore radius ($R^2 = 0.91$, *P*-value = 0.33) [29]. A smaller FB radius indicates better fiber dispersion, leading to smaller

Long *et al. Collagen and Leather*   (2025) 7:6

Page 7 of 13
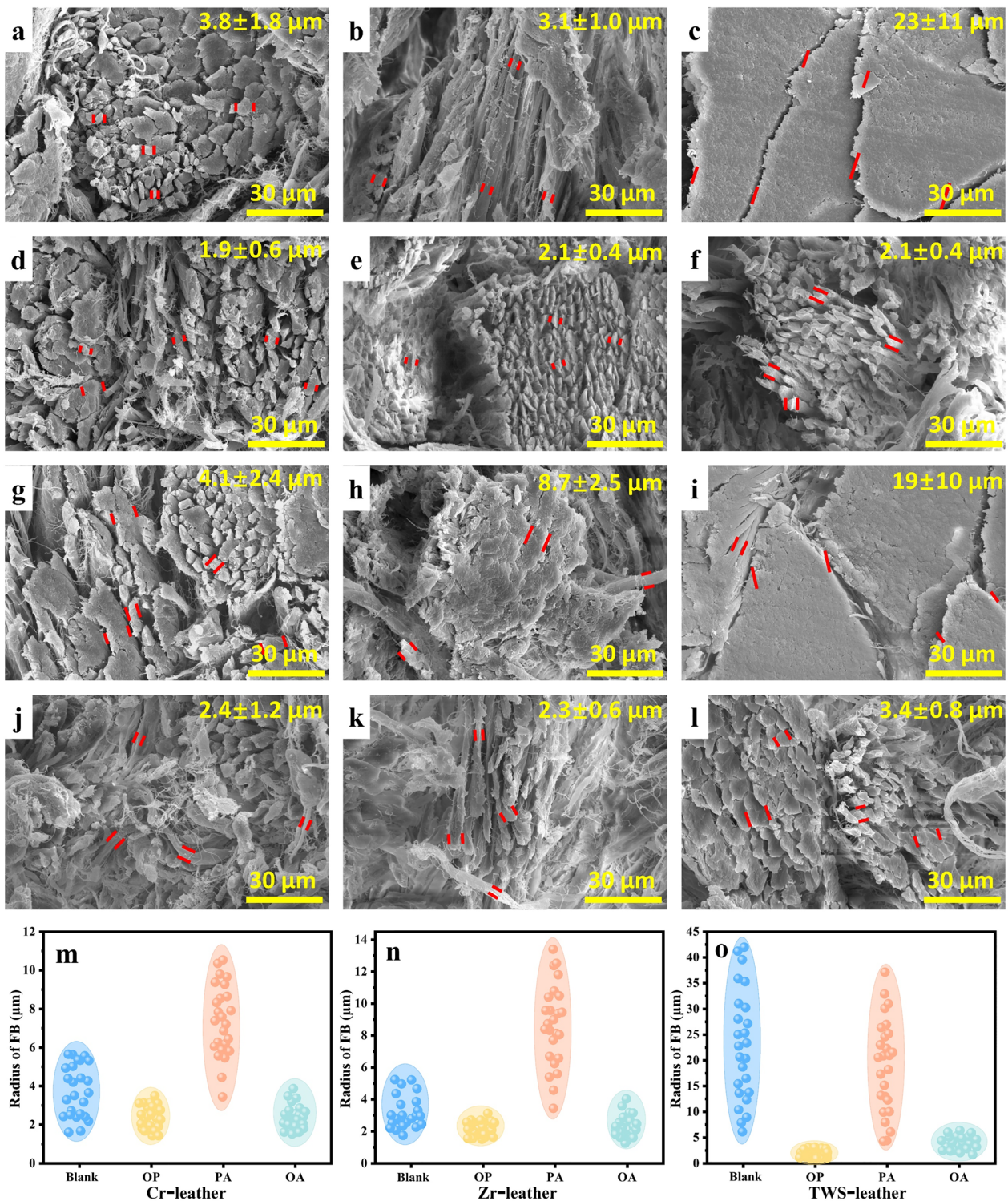
Fig. 3 SEM images of 12 leather samples (1000×): (first column) **a** Cr-leather without fillers and Cr-leather treated with **d** OP, **g** PA and **j** OA; (second column) **b** Zr-leather without fillers and Zr-leather treated with **e** OP, **h** PA and **k** OA; (third column) **c** TWS-leather without fillers and TWS-leather treated with **f** OP, **i** PA and **l** OA. FB radius distributions of **m** Cr-, **n** Zr- and **o** TWS-leathers

Long *et al. Collagen and Leather* (2025) 7:6

Page 8 of 13
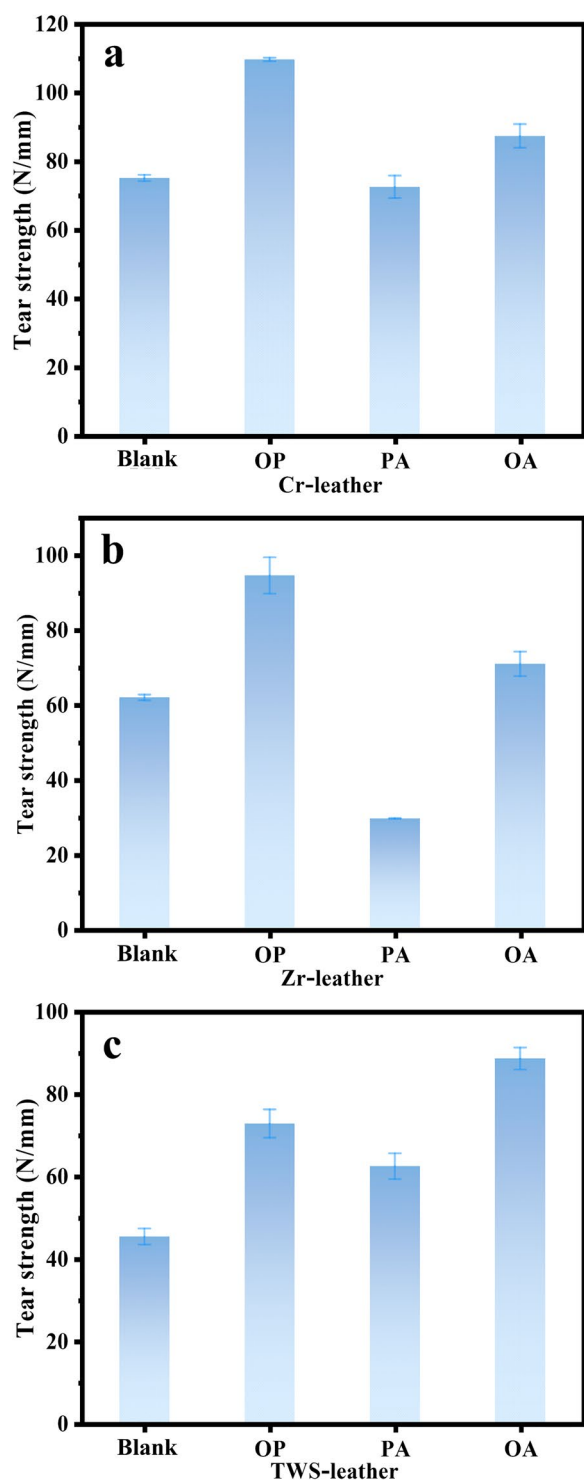
Fig. 4 Tear strength of **a** Cr-, **b** Zr- and **c** TWS-leathers treated with different fillers

pores among FBs and shorter distances between them. In addition, a smaller FB radius results in a larger surface area. When an FB is subjected to loading and begins to slide, the increased internal stress induced by friction

hinders this sliding, thereby improving the mechanical properties.

The experimental TS values of the three leather samples (Cr-, Zr- and TWS-leathers) are correlated with the FB radius obtained from Eq. (9) of the crack-bridging model. Notably, TS is linearly correlated with $(1 − P)/R$ ($R^2 > 0.99$), as shown in Fig. 6, confirming the rationality of FBs being the elementary unit of mechanical properties in leather materials. The range of $(1 − P)/R$ displays significant variation among the three leather samples, indicating differences in their fibrous microstructures. For example, the $(1 − P)/R$ values are 0.0011–0.0018 nm^{-1} for Cr-leather, 0.0005–0.0013 nm^{-1} for Zr-leather and 0.0004–0.0010 nm^{-1} for TWS-leather. Additionally, the value of k is affected by the crosslinking agent and follows this order: $Cr(III) < TWS < Zr(IV)$. Thus, TS demonstrates varying levels of sensitivity to different fibrous structures. Overall, Cr(III) results in a narrow $(1 − P)/R$ range and low sensitivity, contributing to the excellent performance of Cr-leather and highlighting the unique position of Cr tanning technology in the leather industry.

3.4 Regulating the fibril bundle radius
3.4.1 ATR-FTIR spectroscopy results
Figure 7a–c displays the ATR-FTIR spectra of the 12 leather samples. Although the different fillers do not lead to significant changes in the peak positions of the main functional groups, they substantially impact the peak areas, which generally follow the order: OP > OA > Blank > PA. The peak area serves as a reliable indicator of the content of specific functional groups in collagen fibers [30]. The normalized peak areas of typical groups were calculated using the blank sample of Cr-leather as a reference (detailed data in Table S5).

The broad peak at 3700–3000 cm^{-1} can be divided into four components using Gaussian fitting [30, 31]: free water at 3440 cm^{-1}, bound water at 3210 cm^{-1}, amide A at 3310 cm^{-1} and amide B at 3075 cm^{-1} (Fig. S4). Figure 7d–m displays the normalized peak areas after Gaussian fitting.

Cr-leather exhibits the least variation in absorption, while TWS-leather shows the maximum variation with subsequent addition of filler. OP obviously increases the absorption of all groups, especially $-CH_3$, $-CH_2$ and amide B (3075 cm^{-1}). By contrast, PA clearly decreases the absorption across all groups. OA still enhances the absorption compared with the blank but results in a compromise between the effects of OP and PA. Considering the lack of N elemental in OP and abundant $-CH_2$ in PA, the observed increase or decrease in absorption is attributed to the inherent characteristic groups of leather.

The addition of hydrophobic OP increases exposure of functional groups on the collagen fibers, while the
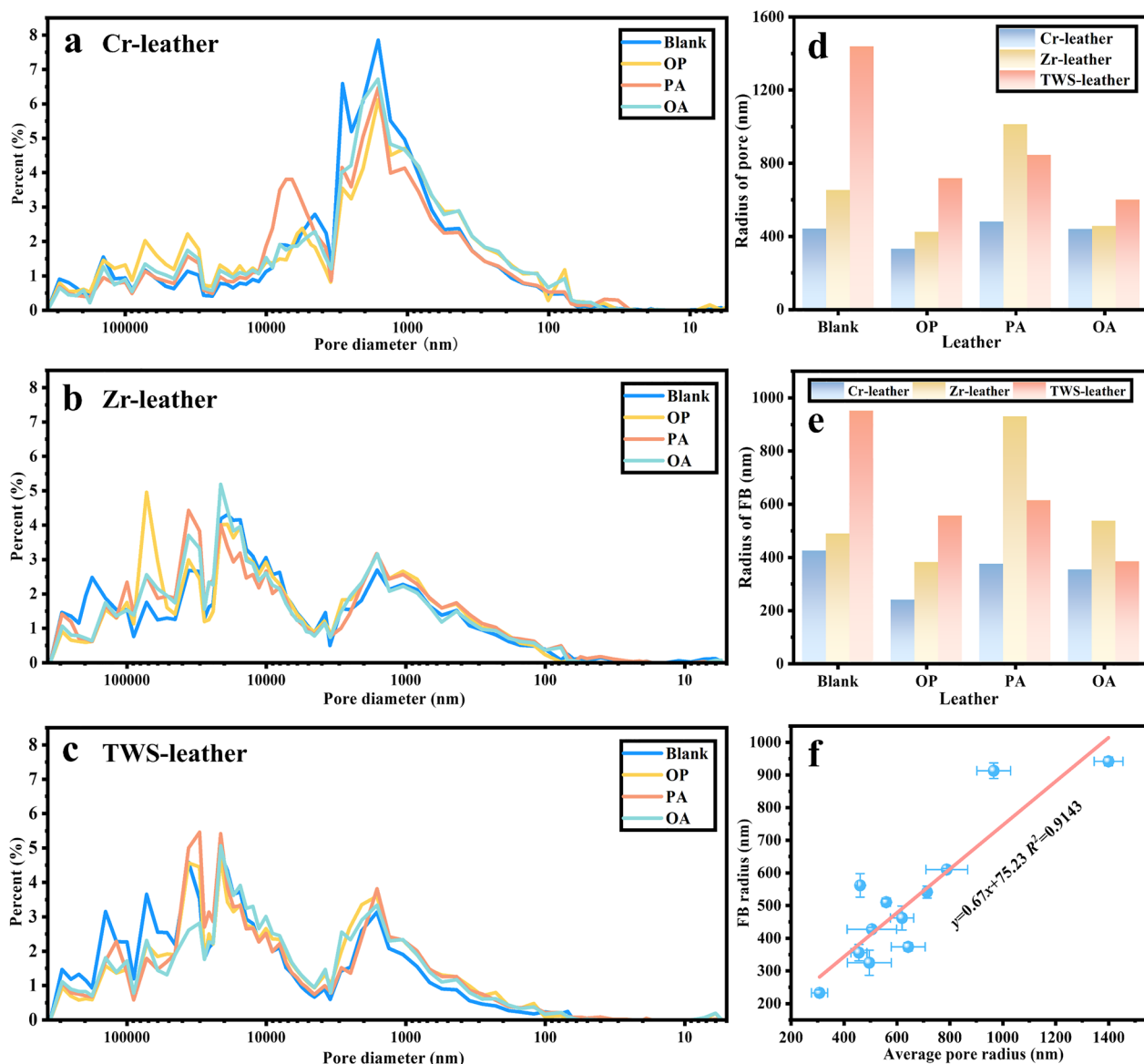
Fig. 5 Pore size distributions of **a** Cr-, **b** Zr- and **c** TWS-leathers treated with different fillers. **d** Average pore radius, **e** FB radius and **f** linear fitting between the average pore radius and FB radius of the leather samples

introduction of hydrophilic PA reduces this exposure. This effect can be ascribed to hydrophobic OP preventing interactions between adjacent fibrils, whereas hydrophilic PA enhances interactions, such as hydrogen bonding, which can mask these groups [32]. OP and PA interact with collagen fibrils at different sites, resulting in an additive effect on the exposure of groups when combined as OA. The extent of group exposure in the collagen fibrils also reflects the aggregation behavior induced by these chemicals. A higher content of exposed groups suggests that more FBs are formed by aggregation, resulting in smaller FB sizes. Thus, hydrophobic OP leads to smaller FBs, while hydrophilic PA promotes the aggregation of fibrils into larger FBs. Ultimately, a smaller FB size indicates better dispersion within the leather sample.

3.4.2 SAXS results

As shown in Fig. 8a–c, the SAXS spectra reveal that Cr- and Zr-leathers exhibit stronger peak signals than TWS leather because the positively charged metal ions effectively increase the electron density of the periodic structure. The D-spacing can be calculated from the peak position as follows [33]:

Long *et al. Collagen and Leather*   (2025) 7:6

Page 10 of 13
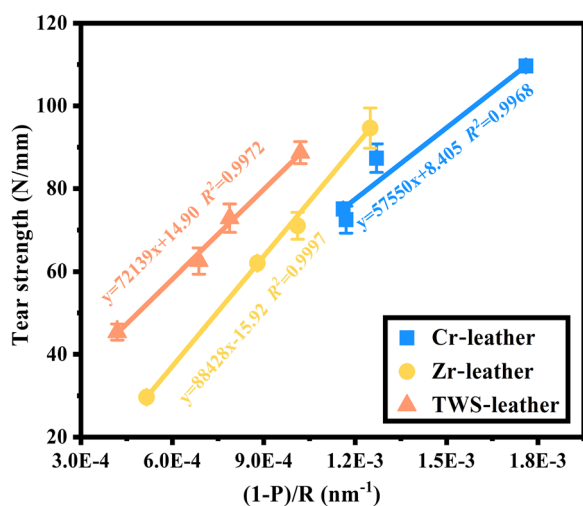
Fig. 6 Fitting of $(1-P)/R$ to the tear strength according to the crack-bridging model

$$d = \frac{2\pi n}{q} \tag{10}$$

where d is the D-spacing (nm), n is the peak order, and q is the scattering vector corresponding to the peak(nm^{-1}). As illustrated in Fig. 8g, the D-spacing follows the sequence of TWS-leather (66.8 nm) > Cr-leather (64.9 nm) > Zr-leather (64.0 nm), indicating that different crosslinking agents affect the quarter staggered arrangement. The addition of the fillers (i.e., OP, PA and OA) does not change the order of the D-spacing for TWS-, Cr- and Zr-leathers. However, the fillers increase the D-spacing by different levels. Notably, OP and OA significantly increase the D-spacing compared to PA. For example, the addition of OP, PA and OA to Cr-leather increases the D-spacing from 64.9 nm to 65.9, 64.9 and 66.8 nm, respectively.

The D-spacing represents the gap between the longitudinal arrangement and overlap regions (Fig. 1), which may reflect the lengths of the fibrils and FBs. The fillers, especially OP and OA, appear to elongate the FBs by regulating the D-spacing, either through stretching the triple helix or by occupying and extending the gap region. According to Eq. (8), longer FBs are associated with increased TS, which supports the experimental results as shown in Fig. 4.

3.4.3 XRD results
XRD was employed to further explore the structural effects of the crosslinking agents and fillers on the leather samples, and the results are shown in Fig. 8d–f. Three distinct peaks are observed in the XRD patterns of all 12 leather samples. The peak at 7°−8° corresponds to the transverse packing spacing of the collagen molecules. The broad peak around 20° represents the hierarchical structure of leather, while the peak at 30° indicates the presence of a triple helix structure [34]. The lateral distance between the collagen molecules and the triple helix pitch were calculated by using diffraction angles of 7°−8° and 30°, respectively:

$$2d \sin\theta = n\lambda \tag{11}$$

where d is the lateral distance between collagen molecules or the helix pitch axial rise distance per residue in nm, θ is the diffraction angle at the peak, n is the diffraction order, and λ is the wavelength of the radiation source ($\lambda = 0.15418$ nm). The relevant results are presented in Fig. 8h, i. Among the crosslinking agents, the lateral distance between the collagen molecules follows this order: Cr-leather (1.25 nm) < Zr-leather (1.26 nm) < TWS-leather (1.27 nm). The addition of fillers reduces the lateral distance and helix pitch to a certain extent, with OP and OA being more effective than PA. For example, the lateral distance for Cr-leather is 1.25 nm, which decreases to 1.22, 1.23 and 1.20 nm after the addition of OP, PA and OA, respectively. Correspondingly, the helix pitch changes from 0.300 nm to 0.297, 0.298 and 0.296 nm, respectively.

A smaller helix pitch indicates that the triple helix is more compressed, which can lead to an increase in the molecular diameter and a reduction in the lateral distance between molecules. This compression suggests a shortening of the triple helix itself. However, the SAXS results show that all the fillers increase the D-spacing. Considering that the D-spacing includes both the gap and overlap regions, these findings indicate that the fillers are likely deposited into the gap region, which not only increases the D-spacing but also elongates the fibrils, thereby improving the TS.

4 Conclusions
In this work, 12 diverse types of leather materials were prepared to investigate the relationship between the aggregation behavior of collagen fibrils and the mechanical properties of the samples. The FBs were identified as the elementary unit governing the mechanical properties of leather, and a straightforward method using MIP was established to measure the FB size. The experimental results showed that the FB size was primarily influenced by the crosslinking agent and could be adjusted by the filler, and a quantitative correlation was established between a smaller FB radius and higher TS. Spectral analysis revealed that hydrophobic fillers exposed more functional groups in the collagen, leading to smaller FB radii and larger FB lengths, which helped fill the gap region between the collagen molecules in the longitudinal

Long *et al. Collagen and Leather*   (2025) 7:6

Page 11 of 13
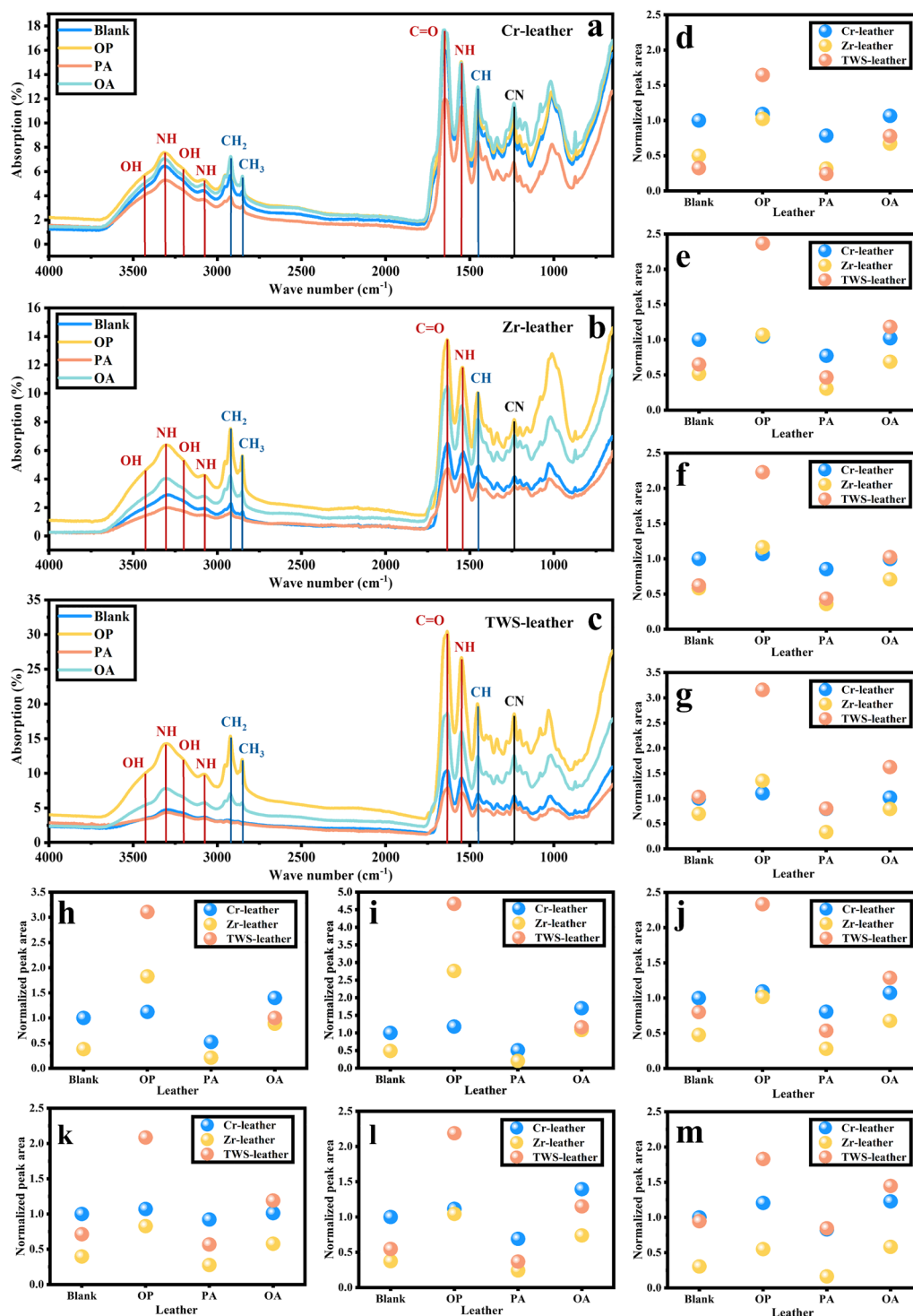
Fig. 7 ATR-FTIR spectra of **a** Cr-, **b** Zr- and **c** TWS-leathers treated with different fillers. Normalization of the functional group peak areas: **d** OH at 3440 cm^{-1}, **e** NH at 3310 cm^{-1}, **f** OH at 3210 cm^{-1}, **g** NH at 3075 cm^{-1}, **h** CH$_2$ at 2935 cm^{-1}, **i** CH$_3$ at 2875 cm^{-1}, **j** C=O at 1650 cm^{-1}, **k** NH at 1550 cm^{-1}, **l** CH at 1450 cm^{-1} and **m** CN at 1240 cm^{-1}
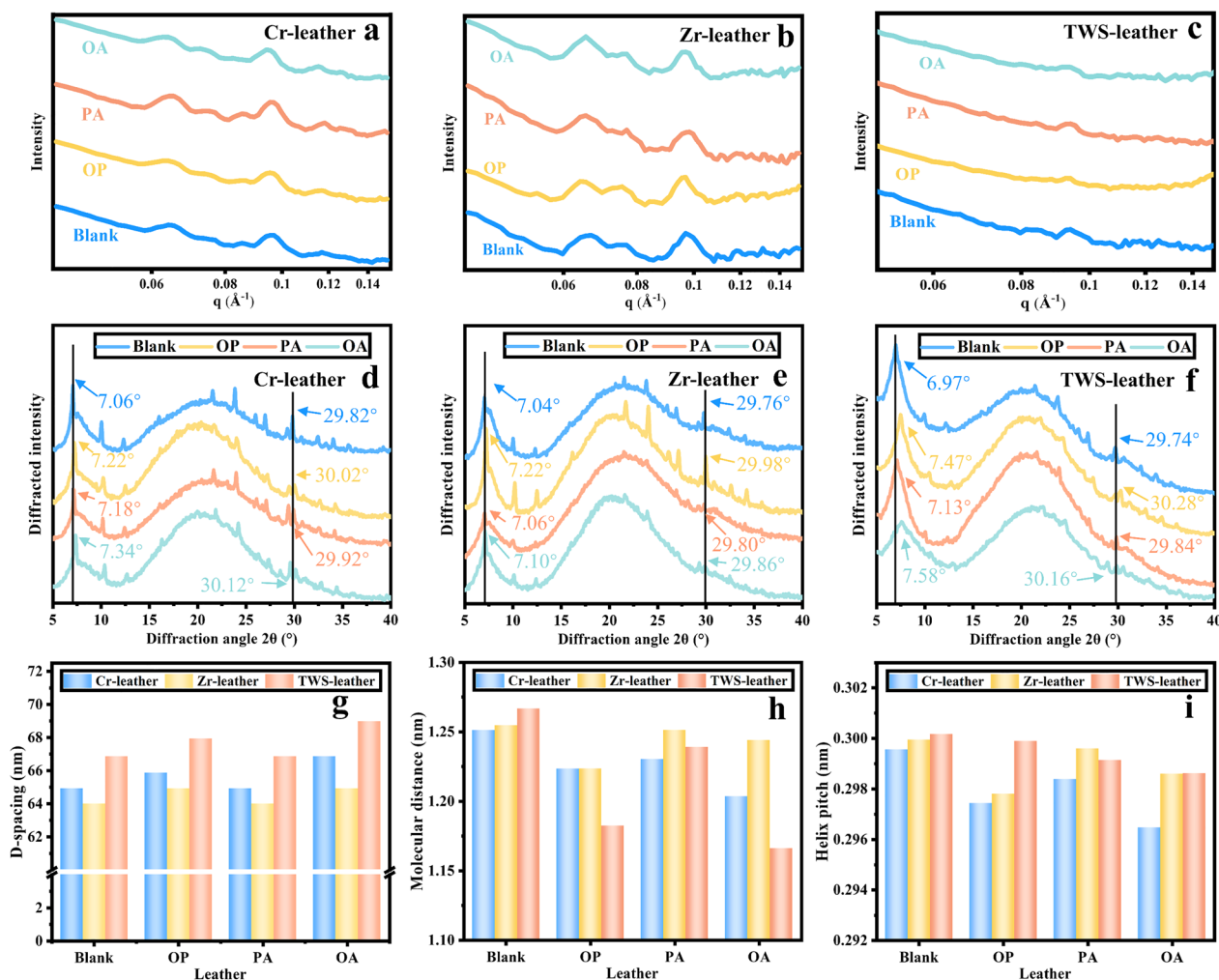
Fig. 8 SAXS results for **a** Cr-, **b** Zr- and **c** TWS-leathers treated with different fillers. XRD results for **d** Cr-, **e** Zr- and **f** TWS-leathers treated with different fillers. **g** D-spacing of fibrils calculated from the SAXS patterns. **h** Lateral distance between the collagen molecules and **i** the triple helix pitch of the 12 leather samples

direction, thereby enhancing TS. Overall, the findings of this study contribute to a better understanding of the mechanical properties of leather materials and can serve as a useful reference for designing fibrous materials with excellent mechanical performance.

Abbreviations
FB   Fibril bundles
MIP   Mercury intrusion porosimetry
OP   Oil phosphate
PA   Polyacrylic acid
SAXS   Small-angle X-ray scattering
SEM   Scanning electron microscopy
TS   Tear strength
XRD   X-ray diffraction

Supplementary Information
The online version contains supplementary material available at https://doi.org/10.1186/s42825-024-00184-4.

Supplementary Material 1

Author contributions
Wenjun Long, Liangqiong Peng, and Jiheng Li conceived this work. Wenjun Long performed and coordinated the experiments and data analysis. Most materials were developed and provided by Yue Yu. Wenhua Zhang acquired the funding for this project. Wenjun Long prepared the manuscript under the supervision of Wenhua Zhang and input from all the authors.

Availability of data and materials

Declarations

Competing interests

The authors declare no conflict of interest.

Author details

[1]National Engineering Laboratory for Clean Technology of Leather Manufacture, Sichuan University, Chengdu 610065, China. [2]Key Laboratory of Leather Chemistry and Engineering of Ministry of Education, Sichuan University, Chengdu 610065, China.

References

1. Choudhary K, DeCost B, Chen C, Jain A, Tavazza F, Cohn R, et al. Recent advances and applications of deep learning methods in materials science. Npj Comput Mater. 2022;8(1):59.
2. China CR, Maguta MM, Nyandoro SS, Hilonga A, Kanth SV, Njau KN. Alternative tanning technologies and their suitability in curbing environmental pollution from the leather industry: a comprehensive review. Chemosphere. 2020;254:126804.
3. Yu Y, Wang H, Wang Y, Zhou J, Shi B. Chrome-free synergistic tanning system based on biomass-derived hydroxycarboxylic acid–zirconium complexes. J Cleaner Prod. 2022;336:130428.
4. Wei C, Wang X, Wang W, Sun S, Liu X. Bifunctional amphoteric polymer-based ecological integrated retanning/fatliquoring agents for leather manufacturing: simplifying processes and reducing pollution. J Clean Prod. 2022;369:133229.
5. Liu X, Wang W, Wang X, Sun S, Wei C. A "Taiji-Bagua" inspired multi-functional amphoteric polymer for ecological chromium-free organic tanned leather production: integration of retanning and fatliquoring. J Clean Prod. 2021;319:128658.
6. Bai Z, Wang X, Zheng M, Yue O, Xie L, Zha S, et al. Leather for flexible multifunctional bio-based materials: a review. J Leather Sci and Eng. 2022;4(1):16.
7. Chen Q, Pei Y, Tang K, Albu-Kaya MG. Structure, extraction, processing, and applications of collagen as an ideal component for biomaterials - a review. Collagen Leather. 2023;5(1):20.
8. He X, Huang Y, Xiao H, Xu X, Wang Y, Huang X, et al. Tanning agent free leather making enabled by the dispersity of collagen fibers combined with superhydrophobic coating. Green Chem. 2021;23(10):3581–7.
9. Covington AD, Wise WR. Tanning Chemistry: The Science of Leather. The Royal Society of Chemistry. 2019. https://doi.org/10.1039/9781839168826.
10. Long W, Peng L, Jiang X, He F, Zhang W. Long-term releasing kinetics of chromium from leather. J Am Leather Chem Assoc. 2021;29(116):437–44.
11. Carlisle CR, Coulais C, Guthold M. The mechanical stress–strain properties of single electrospun collagen type I nanofibers. Acta Biomater. 2010;6(8):2997–3003.
12. Jones B, Tonniges JR, Debski A, Albert B, Yeung DA, Gadde N, et al. Collagen fibril abnormalities in human and mice abdominal aortic aneurysm. Acta Biomater. 2020;110:129–40.
13. Andriotis OG, Desissaire S, Thurner PJ. Collagen fibrils: nature's highly tunable nonlinear springs. ACS Nano. 2018;12(4):3671–80.
14. Long W, Peng L, Li J, Yu Y, Zhang W. On the role of water in regulating the mechanics of collagen fibers. Colloids Surf A Physicochemi Eng Asp. 2024;702:134957.
15. Wells HC, Edmonds RL, Kirby N, Hawley A, Mudie ST, Haverkamp RG. Collagen fibril diameter and leather strength. J Agric Food Chem. 2013;61(47):11524–31.
16. Pei Y, Yang W, Tang K, Kaplan DL. Collagen processing with mesoscale aggregates as templates and building blocks. Biotechnol Adv. 2023;63:108099.
17. Goh KL, Holmes DF, Lu Y, Purslow PP, Kadler KE, Bechet D, et al. Bimodal collagen fibril diameter distributions direct age-related variations in tendon resilience and resistance to rupture. J Appl Physiol. 2012;113(6):878–88.
18. Cherdchutham W, Becker CK, Spek ER, Voorhout WF, Weeren PRV. Effects of exercise on the diameter of collagen fibrils in the central core and periphery of the superficial digital flexor tendon in foals. Am J Vet Res. 2001;62(10):1563–70.
19. Chen Z, Wei B, Mo X, Lim CT, Ramakrishna S, Cui F. Mechanical properties of electrospun collagen–chitosan complex single fibers and membrane. Mater Sci Eng C. 2009;29(8):2428–35.
20. Ji J, Bar-On B, Wagner HD. Mechanics of electrospun collagen and hydroxyapatite/collagen nanofibers. J Mech Behav Biomed Mater. 2012;13:185–93.
21. Li M, Mondrinos MJ, Gandhi MR, Ko FK, Weiss AS, Lelkes PI. Electrospun protein fibers as matrices for tissue engineering. Biomaterials. 2005;26(30):5999–6008.
22. He X, Wang Y, Zhou J, Wang H, Ding W, Shi B. Suitability of pore measurement methods for characterizing the hierarchical pore structure of leather. J Am Leather Chem Assoc. 2019;114(2):41–7.
23. Ke L, Wang Y, Ye X, Luo W, Huang X, Shi B. Collagen-based breathable, humidity-ultrastable and degradable on-skin device. J Mater Chem C. 2019;7(9):2548–56.
24. QB/T 2711–2005. Leather—Physical and mechanical tests—Determination of tear load—Double edge tear. 2005.
25. Meng Q, Li B, Li T, Feng XQ. Effects of nanofiber orientations on the fracture toughness of cellulose nanopaper. Eng Fract Mech. 2018;194:350–61.
26. Meng Q, Li B, Li T, Feng XQ. A multiscale crack-bridging model of cellulose nanopaper. J Mech Phys Solids. 2017;103:22–39.
27. Haslach HW. Time-dependent mechanisms in fracture of paper. Mech Time-Depend Mater. 2009;13(1):11.
28. Yao Q, Wang Y, Chen H, Huang H, Liu B. Mechanism of high chrome uptake of tanning pickled pelt by carboxyl-terminated hyper-branched polymer combination chrome tanning. Chem Sel. 2019;4(2):670–80.
29. Deshmukh GP, Ravindra MR, Jose N, Wasnik PG, Dhotre AV. Moisture sorption behavior and thermodynamic properties of dry-crystallized Palada payasam (rice flakes milk pudding) mix determined using the dynamic vapor sorption method. J Food Process Preserv. 2020. https://doi.org/10.1111/jfpp.14819.
30. Kudo S, Ogawa H, Yamakita E, Watanabe S, Suzuki T, Nakashima S. Adsorption of water to collagen as studied using infrared (IR) microspectroscopy combined with relative humidity control system and quartz crystal microbalance. Appl Spectrosc. 2017;71(7):1621–32.
31. Kudo S, Nakashima S. Water retention capabilities of collagen, gelatin and peptide as studied by IR/QCM/RH system. Spectrochim Acta Part A Mol Biomol Spectrosc. 2020;241:118619.
32. Zou X, Lan Y, Li Z, Zhan X. Effects of polyacrylic acid on the structure of collagen fibre. J Soc Leather Technol Chem. 2014;1(98):172–6.
33. Zhang Y, Ingham B, Cheong S, Ariotto N, Tilley R, Naffa R, et al. Real-time synchrotron small-angle x-ray scattering studies of collagen structure during leather processing. Ind Eng Chem Res. 2018;57(1):63–9.
34. Zhu S, Gu Z, Xiong S, An Y, Liu Y, Yin T, et al. Fabrication of a novel bio-inspired collagen-polydopamine hydrogel and insights into the formation mechanism for biomedical applications. RSC Adv. 2016;6(70):66180–90.

Publisher's Note